


Zwitterionic Bergman cyclization triggered polymerization gives access to metal-graphene nanoribbons using a boron metal couple

Dinesh V. Vidhani¹, Rosemary Ubeda¹, Thalia Sautie¹, Diana Vidhani² & Manoharan Mariappan³

With the rapid growth in artificial intelligence, designing high-speed and low-power semi-conducting materials is of utmost importance. This investigation provides a theoretical basis to access covalently bonded transition metal-graphene nanoribbon (TM-GNR) hybrid semiconductors whose DFT-computed bandgaps were much narrower than the commonly used pentacene. Systematic optimization of substrates containing remotely placed boryl groups and the transition metals produced the zwitterions *via* ionic Bergman cyclization (*i-BC*) and unlocked the polymerization of metal-substituted polyenynes. Aside from *i-BC*, the subsequent steps were barrierless, which involved structureless transition regions. Multivariate analysis revealed the strong dependence of activation energy and the cyclization mode on the electronic nature of boron and Au(I). Consequently, three regions corresponding to radical Bergman (*r-BC*), ionic Bergman (*i-BC*), and ionic Schreiner-Pascal (*i-SP*) cyclizations were identified. The boundaries between these regions corresponded to the mechanistic shift induced by the three-center-three-electron (3c-3e) hydrogen bond, three-center-four-electron (3c-4e) hydrogen bond, and vacant p-orbital on boron. The ideal combination for cascade polymerization was observed near the boundary between *i-BC* and *i-SP*.

¹Department of Math & Natural Science, Miami Dade College, Miami Dade College, 627 SW 27th Ave, Miami, FL 33135, USA. ²Miami Dade Virtual School, 560 NW 151st, Miami, FL 33169, USA. ³Department of Natural Science North Florida College, 325 Turner Davis Dr, Madison, FL 32340, USA.
email: dvidhani@mdc.edu

As we reach the quantum limit of silicon-based semiconductors, graphene-based materials have become the focus of intense research due to their applications in solar cells^{1,2}, OLEDs³, bioengineering^{4,5}, drug and gene delivery systems^{6,7}, composite materials⁸, and energy storage devices^{9,10}. Despite their extraordinary mechanical and optoelectronic properties, vanishing bandgaps in graphene limits its ability to replace silicon-based semiconductors. Graphene nanoribbons (GNRs), which are quasi-one-dimensional polyacene sheets with a width of less than 100 nm and a bandgap between 1–1.6 eV, offer a better solution to the shortcomings of silicon and graphene-based materials (Fig. S1 in SI)¹¹. The structure and material properties of graphene nanoribbons (GNRs) depend heavily on the method of synthesis. For example, the electronic properties of GNRs with jagged edges created using electron-beam lithography differ from the more precise armchair or zigzag GNRs made using a bottom-up technique utilizing polycyclic molecules¹². In this context, linearly fused polyaromatic hydrocarbons (PAH) with a general formula $C_{4n+2}H_{2n+4}$ are essential precursors for synthesizing GNRs and serve as molecular models to understand their material properties (Fig. S1 in SI)¹³. However, the linear structure of acenes contains a single Clar or aromatic sextet (six π -electrons), making them susceptible to oxidation or polymerization and challenging to synthesize, especially when the number of rings is high^{14–19}. Hence, producing these molecules using traditional synthetic organic methods has been difficult²⁰. Making metal-hybrid polyacene materials is even more complex and requires special techniques (Fig. 1). These materials are predicted to have a combination of GNRs and pure metals properties, especially if the distance between the covalently bonded metal atoms closely matches the metallic bond distance in the pure metal.

Among various methods, Bergman cyclization (BC) provides a convenient strategy for synthesizing a wide range of fused polyaromatic compounds, such as substituted rylene. Mechanistically, BC can be seen as a two-step, high activation energy pericyclic rearrangement, with an unstable diradical intermediate between the two transition states for ring formation and opening (Fig. 2). Roth et al. experimentally corroborated Bergman's prediction of high activation energy, with a measured ΔH^\ddagger of 28.7 ± 0.5 kcal/mol at 200 °C^{21–23}. This is because, unlike a concerted pericyclic process, the number of bonds broken and formed in the cycloaromatization step are not conserved, leading to the formation of a six-membered aromatic diradical that is orthogonal to the aromatic π -system and cannot take advantage of adjacent conjugated systems (Fig. 2, top left). As a result, this

diradical is highly reactive and can produce a range of fused cycloaromatic compounds, yet it often gives low yields, 5-endo products (Fig. 2, bottom left), or reduced products. To overcome these limitations, the exploration of ionic-BC is essential^{24–29}. In a recent study, Hashmi *et al.* found that 5-endo cyclization of dual σ, π -Au(I) substituted enediynes led to a non-aromatic fulvenylene cation (Fig. 2, top right)^{30,31}. This route is comparable to Schreiner–Pascal (SP) cyclization; however, the classic SP cyclization is not preferred due to its high activation energy³² and the formation of non-aromatic fulvene diradicals (Fig. 2, bottom left)³³, which is not a feature of the dual σ, π -Au(I)-catalyzed protocol. Subsequently, Alabugin *et al.* explored the dual σ, π -Au(I)-catalyzed Bergman cyclization, providing valuable insights into the nature of 1,4-zwitterionic species^{34–37}.

From this viewpoint, we envisioned polyenyne containing tunable σ -Au(I)-acetylide and boryl groups to undergo the desired cascade polymerization with high 6-endo selectivity (Fig. 2, bottom right). Previous studies have shown that the potential energy surface (PES) of concerted pericyclic rearrangements can be altered by the influence of transition metals or frustrated Lewis pairs (FLPs), leading to an interrupted or aborted process (Fig. 3)³⁸. Notably, Au(I)-catalyzed Claisen rearrangements of allenyl vinyl ethers and propargyl vinyl ethers appear to be switching from a concerted to a stepwise pathway (Fig. 3B). The near-perfect alignment of $\sigma^*(C3-O)$ and $\sigma(C2-Au)$ at the second transition state (TS2), which manifests as an inflection on the PES, corroborates this phenomenon^{39–43}. Alternatively, the Cope rearrangement mediated by the FLPs can be interrupted by a zwitterionic intermediate in which the boryl group holds onto the electron density it acquired, thus slowing down or aborting $\sigma(C3-C4)$ bond scission (Fig. 3C, D). The present work aimed to explore the capability of zwitterions in (BC), and the stereoelectronic effects it can have on the cascade cyclization of polyenyynes leading to metal-polyacene semiconducting materials. An extensive DFT analysis helped to design the polyenyne substrates that contained the ideal combination of a boryl group and Au(I)L and enabled the polyenyynes to undergo a zwitterionic BC reaction without any side reactions. Further, the calculated HOMO-LUMO gaps and reorganization energies of the resulting transition metal-polyacene hybrid material were comparable to popular p-type semiconductors, such as pentacene.

Results and discussion

The polyenyynes for the present investigation contain three major components (1) the boryl group, (2) a covalently bonded

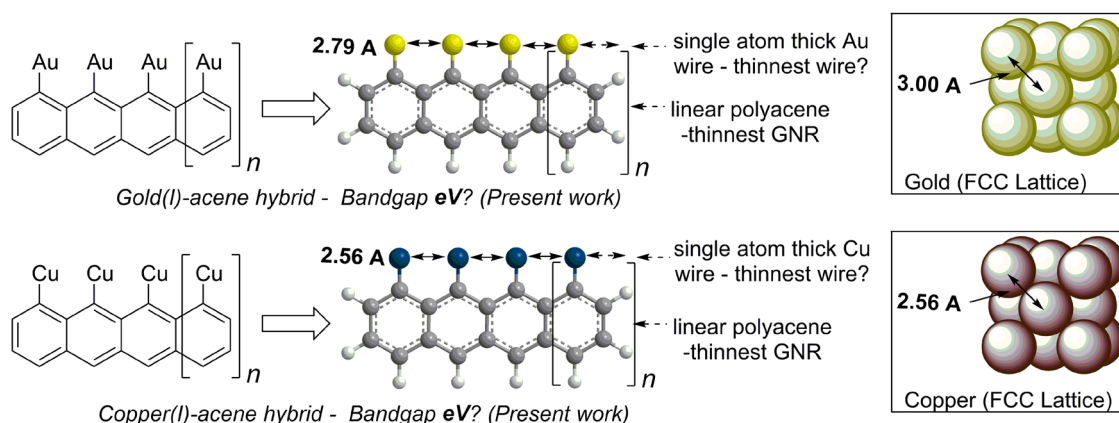


Fig. 1 This figure illustrates a proposed metal-polyacene hybrid semiconductor created through ionic BC-triggered cascade polymerization. It displays the thinnest linear polyacene covalently bonded to a single-atom-thick transition metal wire, with the distance between metal atoms similar to that of the face-centered cubic lattice of gold and copper crystals.

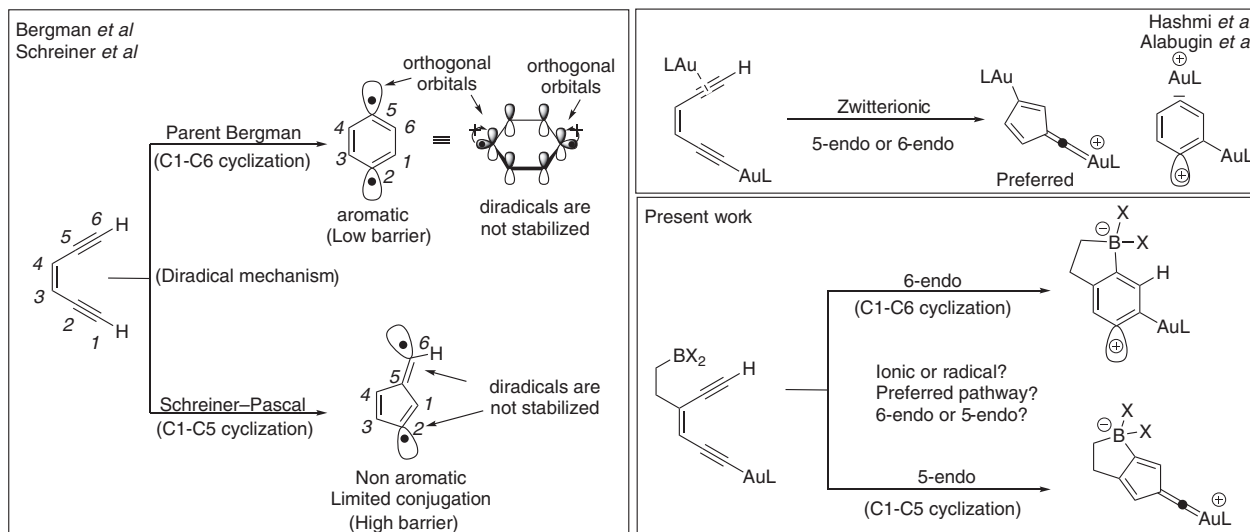


Fig. 2 Possible outcomes in the cyclization of enediynes. The left box shows the conventional C₁-C₆ Bergman (BC) and C₁-C₅ Schreiner-Pascal (SP) cyclizations giving diradicals. The top right depicts the dual Au(I)-catalyzed zwitterionic version of BC, and the bottom right box shows the present work on the boron-Au(I) triggered zwitterionic BC and SP cyclizations.

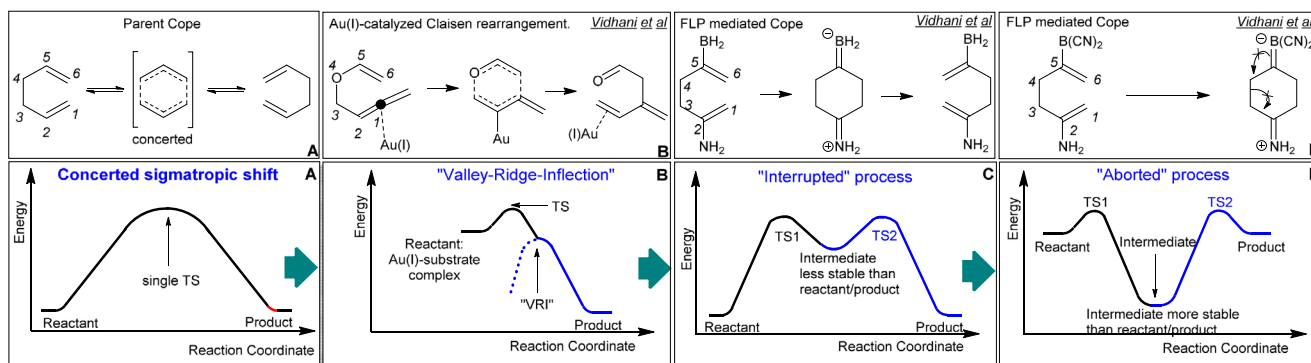


Fig. 3 Evolution of concerted potential energy surface (PES) into interrupted and aborted pathways. **A** Parent Cope rearrangement, **B** Au(I)-catalyzed Claisen rearrangement displaying inflection along the PES, **C** FLP-mediated interrupted Cope rearrangement, and **D** FLP-mediated aborted Cope rearrangement.

transition metal with the alkyne, and (3) the repeating polyenyne motifs. We hypothesized that the boryl groups play a critical role in controlling the barrier, deciding the 5-endo/6-endo selectivity, and selecting between radical and zwitterionic pathways. Based on the recent independent studies by the Alabugin and Hashmi groups, we further theorized that the electronic nature of Au(I)-acetylide would affect the stability of the developing sp^2 -hybridized β -carbocation at C2 of enediyne (Fig. 2). However, for the success of this strategy, it was essential that the effect of Au(I)-acetylide was synergic to the boryl group in the multistep cascade polymerization. Thus, before analyzing the cascade process, we investigated the role of ligand on Au(I) (Fig. 4B), the substituents on the boryl group (Fig. 4C), and the combined effect of Au(I) (Fig. 4D) and boryl groups on the overall nature of BC in substituted enediynes (Fig. 4E).

Bergman cyclization of Au(I)-substituted enediynes. Previous studies of BC have shown a strong agreement between experimental kinetics and the data obtained using several theoretical methods, including CCSD(T), CASSCF, CASPT2, MBPT, and various DFT approaches^{44–48}. In particular, the combination of experimental and computational studies demonstrated the capability of B3LYP and PBE0 methods to accurately predict the activation barriers of pericyclic rearrangements such as Bergman

cyclizations, Cope rearrangement, Claisen rearrangement, and several transition metal-catalyzed reactions^{33,37,38,40,45}. In the present study, the activation enthalpies for parent BC were found within 1 kcal/mol of experimentally determined barrier (32 kcal/mol, Table S1 in SI and Supplementary Data 1) when using B3LYP/LANL2DZ and PBE0/6-311+G**/def2-TZVP methods. Although both methods were dependable, the former was selected due to its reliability and affordability in predicting the properties of the compounds containing heavy atoms such as Au(I), Cu(I), and Br. From the mechanistic perspective, the parent enediynes and the systems containing σ -Au(I)-acetylides adopted a classical BC, generating 1,4-diradical *via* aromatic transition states [NICS(1): -11.0 ppm] and the activation energies ranging from 32–34 kcal/mol (Table S1 in SI). As for the ligands on Au(I), the fluoride ion showed the lowest barrier, followed by trimethyl phosphine and water (Table S1 in SI). The NBO analysis of the three transition states revealed that the radical stabilizing interaction from the remotely placed fluoride was far greater than trimethyl phosphine and water (Fig. 5). Furthermore, as evidenced by the interaction energies [48.2 kcal, Fig. 5], the fluoride ion enhances the orbital overlap between terminal carbon atoms and facilitates the formation of σ (C1–C6) bond. A similar radical stabilizing interaction is observed for water and trimethyl phosphine ligands, but the effect was not as pronounced (Fig. 5).

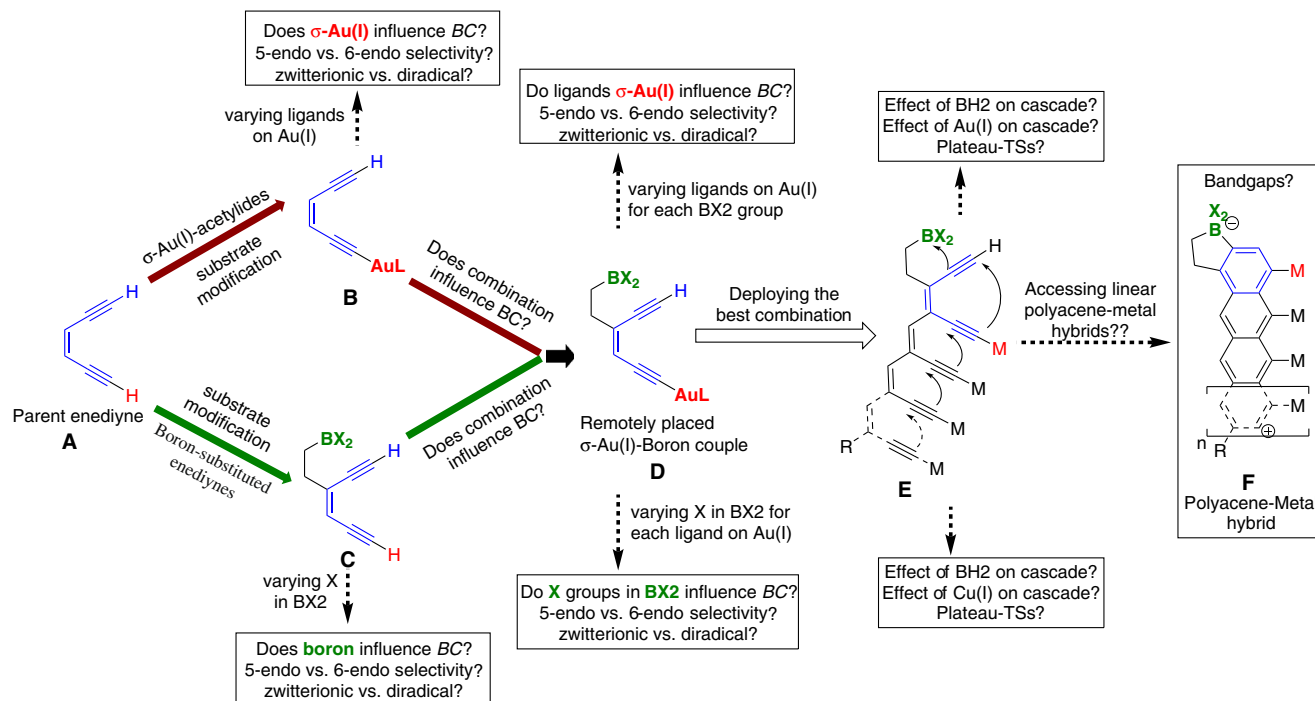


Fig. 4 The flow chart provides a logical evolution of substrates from the parent enediyne into multifaceted polyenyne that can form polyacene-metal hybrids. Each modification in the substrate design was investigated separately using DFT level calculations [A (Parent enediyne) → D (Au/boron couple)]. Structures B and C correspond to mono σ-Au(I) and mono boryl substituted enedynes. Structure E corresponds to the polyene containing the best combination of Au(I)/boryl couple. Structure F corresponds to the metal-substituted polyacenes product.

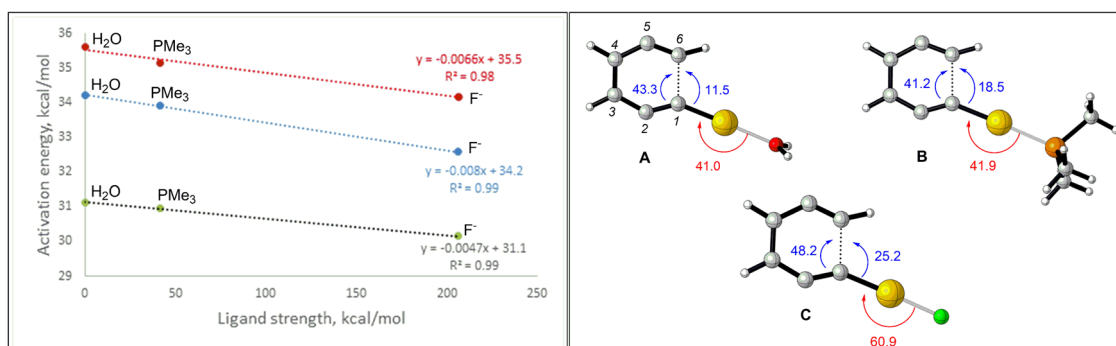


Fig. 5 Plot on the left shows the dependence of activation energy on the strength of the ligand. Red, blue, and gray dotted lines in the plot correspond to the activation energies calculated at the B3LYP/6-311+G**/def2-TZVP, B3LYP/LANL2DZ, and PBE0/6-311+G**/def2-TZVP levels respectively. Structures A, B and C on the right correspond to the transition state geometries of substrates consisting of H₂O, PMe₃, and F⁻ attached to the Au(I)-acetylide, respectively. The values in red and blue correspond to interaction energies expressed in kcal/mol.

The results to this point suggest that the ligands bound to σ-Au(I)L-acetylide do not alter the radical nature of the intermediate or the C1–C6 endo-selectivity of the enediyne substrates. Alabugin et al. demonstrated that this outcome might significantly change upon adding the second Au(I) that coordinates with the π(C5–C6) bond. The two Au(I) motifs in such dual σ,π-Au(I) activation produce stereoelectronically-stabilized zwitterion (Fig. 2)³³. The energy of this trajectory was 16 kcal/mol lower than the 1,4-diradical pathway (Table S1 in SI). Conceptually, the TS of a pericyclic rearrangement can be visualized as the saddle point in a continuous spectrum spanned between the homolytic and the heterolytic bond-altering processes^{49–51}. In the present study, the near-zero NBO charges at C2 and C5 of the parent enediyne and mono σ-Au(I) substrates clearly indicated the formation of aromatic 1,4-diradicals through

homolytic bond-altering processes (Fig. 6A, B). The aromatic character of these radicals was confirmed by NICS (1) [Parent BC: –12.5 ppm; mono-Au(I) BC: –12 ppm]. However, the electrostatic repulsion between C1 and C6, as evidenced by their NBO charge distribution, contributed to the high activation energies in parent and mono-Au(I) systems (Fig. 6A, B).

In contrast, the dual σ,π-Au(I) BC was characterized by an early non-aromatic-TS [NICS (1) = –5.2 ppm] where the NBO charges at C1 and C6 enabled the formation of σ-(C1–C6) bond (Fig. 6C). As previously demonstrated in Au(I)-catalyzed Claisen rearrangements (Fig. 3B), the potential energy surface (PES) of this reaction too exhibited a valley ridge inflection (VRI) along the IRC (Fig. 7, right)^{52–56}. The C2–C6 and C1–C6 bond distances at the VRI further suggest that the 5-endo cyclization and 6-endo BC pathways bifurcate at the VRI and that they share

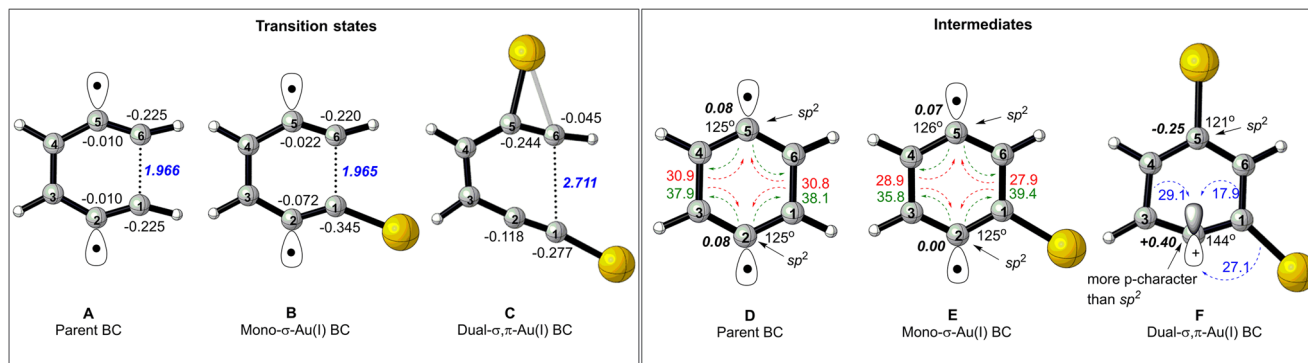


Fig. 6 Bergman cyclization of parent enediyne, mono-Au(I)-acetylide, and dual Au(I)-catalyzed systems. Left: Transition state geometries of BC in parent enediyne (A), mono-Au(I)-acetylide system (B), and dual Au(I)-catalyzed system (C) obtained at the B3LYP/LANL2DZ level. Values in black and blue fonts reflect the NBO charges and the C1-C6 distance, respectively. Right: Geometries corresponding to the parent BC (D), mono- σ -Au(I) BC (E), and dual σ,π -Au(I) BC (F) intermediates. Values and arrows in red correspond to the interaction energies when σ (C1-C6) and σ (C3-C4) bonds are symmetrically delocalized into the antibonding orbital of closed shell C2-C5 diradical. Values and arrows in green reflect interaction energies when diradical is symmetrically delocalized into σ^* (C1-C6) and σ^* (C3-C4) bonds. Values and arrows in blue reflect interaction energies when σ (C1-C6), σ (C3-C4), σ (C1-Au) bonds are delocalized into the empty *p*-orbital of carbocation at C2.

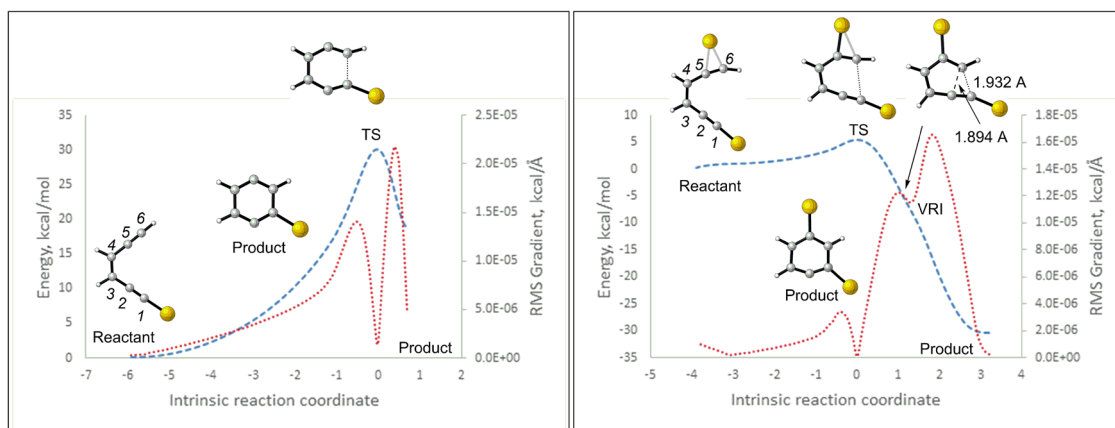


Fig. 7 Comparison of the IRC paths for the mono-Au(I)-acetylide (left) and dual Au(I)-catalyzed system (right). Calculations were performed at the B3LYP/LANL2DZ level. The dashed blue line and dotted red line correspond to energy changes and RMS gradient along the intrinsic reaction coordinate. VRI corresponds to “Valley Ridge Inflection”⁵¹⁻⁵⁵.

a common non-aromatic-TS. Hence, several experimental studies have shown the formation of the fulvene-type intermediate from the Au(I)-catalyzed 5-endo cyclization of enediynes^{30,31,33}.

We then compared the 6-endo cyclization (BC) products of mono-Au(I), dual σ,π -Au(I), and parent BC pathways. For parent BC, a slight increase in $\angle C1C2C3$ and $\angle C4C5C6$ from 120° to 125° suggested higher *p*-character at C2 and C5 of 1,4-diradical intermediate (Fig. 6D). These out-of-plane diradicals were stabilized by a strong and symmetrical two-way interaction with adjacent σ -bonds (Fig. 6D). Similarly, the NBO charges, hybridization, and geometry at C2 and C5 of the σ -Au(I)-acetylide system (Fig. 6E) suggested the presence of a 1,4-diradical intermediate, as seen in the analogous parent BC product (Fig. 6D). In contrast to the parent BC and the σ -Au(I)-acetylide system, the dual σ,π -Au(I)-catalyzed BC activates the π (C5-C6) bond, leading to heterolytic cleavage and formation of zwitterions that are stabilized by two Au(I) ions. There is a noteworthy increase in the bond angle of the sp^2 -hybridized C2 carbon atom, which allows electron density to flow from σ (C1-C6) and σ (C3-C4) to carbocation at C2, thus stabilizing it (Fig. 6F). Although DFT studies point to the formation of an aromatic zwitterion [NICS(1): -12.7 ppm], Hashmi et al. carried out experiments that show a preference for a non-aromatic fulvene-type zwitterion generated via 5-endo cyclization

(Fig. 2)^{30,31}. In this context, the first study predicts that the mono σ -Au(I)acetylides do not affect the nature of the intermediate if used without second π -(C5-C6)-coordinated Au(I) (Figs. 6, 7). We thus propose a novel strategy based on a boron-Au(I) couple, which would enable boryl groups to activate π -(C5-C6) towards 6-endo ionic BC, and σ (C1-Au(I)) would offer stability to the β -carbocation at C2 (Fig. S4 in SI and Fig. 2).

Boron-mediated Bergman cyclization. Conceptually, Bergman cyclization is considered an interrupted version of Cope rearrangement where a high energy 1,4-diradical intermediate interrupts a concerted pericyclic process (Fig. 2, left)^{49,50}. In the present context, we predicted the boryl groups would activate the π (C5-C6) bond in enediynes, resulting in a BC cyclization analogous to the π -Au(I)-catalyzed BC³³. For the model substrates, B3LYP and PBE0-computed activation energies strongly correlated with the electrophilicity of the boryl groups (Table S2 in SI and Fig. S2 in SI). The NBO charge analysis and the high activation energy (32 kcal/mol) for the substrates containing electron-rich $-B(NH_2)_2$ group indicated a diradical pathway (Table S2 in SI). In contrast, the $-B(CN)_2$ group showed a zwitterionic trajectory and a low activation energy of 14.6 kcal/mol, similar to mono π -Au(I)-catalyzed BC systems³³.

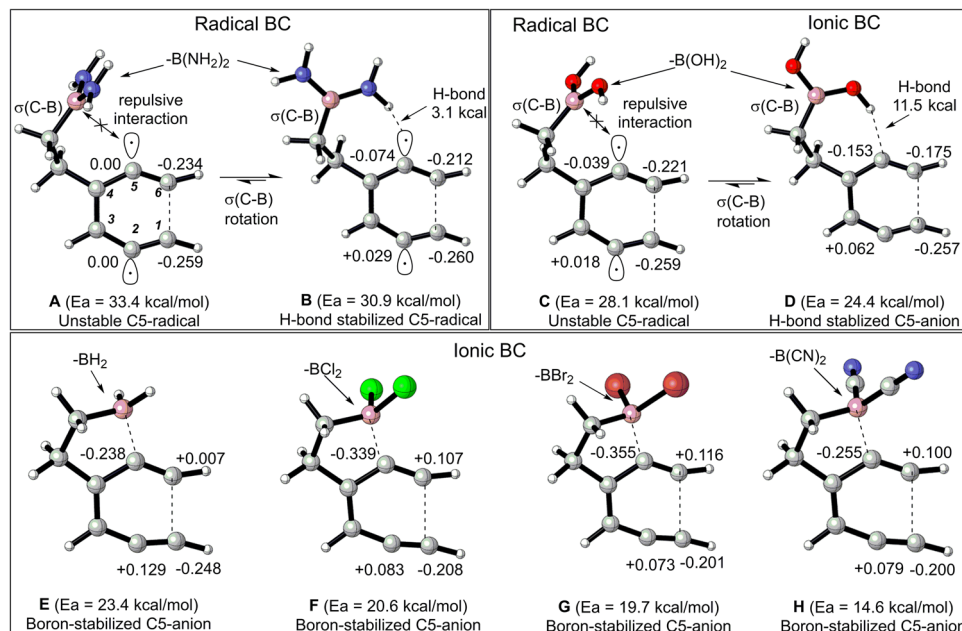


Fig. 8 B3LYP/LANL2DZ-optimized transition state geometries of substrates containing electronically diverse boryl groups. Structures **A** and **B** correspond to non hydrogen bonding and hydrogen bonding transition states in $-\text{B}(\text{NH}_2)_2$ substituted substrates respectively, Structures **C** and **D** correspond to non hydrogen bond and hydrogen bonding transition states in $-\text{B}(\text{OH})_2$ substituted substrates respectively. Structures **E**, **F**, **G**, and **H** correspond to the transition states of substrates containing $-\text{BH}_2$, $-\text{BCl}_2$, $-\text{BBr}_2$, and $-\text{B}(\text{CN})_2$ groups respectively. The values reflect the NBO charges at C1, C2, C5, and C6 carbons.

A broader selection of substituents on the boryl groups showed a similar trend at the B3LYP/LANL2DZ level (Fig. 8). These substituents were selected based on Hammett's constants, indicative of their ability to modify the electron density in the empty $2p$ orbital of the boron atom (See Fig. S3 in SI for the ESP maps). Based on the transition state geometries and NBO charges at C1, C2, C5, and C6, three main types of transition states were identified: (1) classic BC -type TS, (2) H bond stabilized TS, and (3) boron-stabilized TS. Substrates containing electron-rich $\text{B}(\text{NH}_2)_2$ and $-\text{B}(\text{OH})_2$ groups exhibited the classic BC -type TS with a high activation energy. The delocalization of non-bonding electrons on the amino and hydroxy groups partially filled the $2p$ orbital on boron and prevented it from interacting with the newly developed radical center at C5 (Fig. 8A, C). However, the rotation of the $\sigma(\text{C-B})$ bond enabled the amino and the hydroxy groups on boron to form a 3-center-3-electron ($3c-3e$) and 3-center-4-electron ($3c-4e$)-hydrogen bond with the intermediate at C5 respectively. The $3c-3e$ interaction of the C5 radical with the amino group is unique, as it forms a hydrogen bond instead of abstracting hydrogen atoms from the amino group. For a more efficient H bond donor, such as $-\text{OH}$ on boron (Fig. 8C, D), we observed a mechanistic shift from a high-energy radical BC -type pathway (28.4 kcal/mol) to a lower-energy zwitterionic BC pathway (24.4 kcal/mol). As for the boron-stabilized TS, the NBO charges showed a developing zwitterion at C2 and C5, where the vacant $2p$ orbital on boron strongly interacted with the developing carbanionic center at C5 (Fig. 8E–H). The charges at C1 and C6 carbons further enabled the formation of a $\sigma(\text{C1-C6})$ bond and facilitated the flow of electron density from $\pi(\text{C1-C2})$ bond to vacant $p(\text{boron})$ via $\pi^*(\text{C6-C5})$, making the TSs of these substrates more polar than their diradical counterparts (Fig. 8E–H). Additionally, Hammett's constants of the substituents and dipole moment of the TS were negatively correlated with the activation barrier, indicating the role of electrophilic boron in shifting the reaction towards zwitterionic intermediates through a highly polar transition state (Fig. 9).

Overall, the boron-mediated BC approach is more reliable and efficient than the π -coordinated $\text{Au}(\text{I})$ -catalyzed method, as it did not show any undesired 5-endo cyclization in any of the three pathways discussed.

Combining two pieces together: synergetic effect of the boryl group and σ - $\text{Au}(\text{I})$ -acetylide complex on the Bergman cyclization. The combination of electron-deficient boryl group and electron-rich σ - $\text{Au}(\text{I})$ -acetylide can form a frustrated Lewis pair (FLP) if placed remotely in the same enediyne. In such cases, the intervening sp^3 -hybridized methylene groups restrict the typical quenching of Lewis pairs, and Bergman cyclization provides an alternate route to share the electron density between them through σ -bonding, as illustrated in Fig. 10.

This model is similar to the former study in which boron-mediated [3,3] and [1,5]-sigmatropic shifts helped to establish direct resonance-enabled communication between the remotely situated donor and acceptor groups (Fig. 10)^{37,41}. Generally, enediynes prefer Bergman cyclization over the Schreiner–Pascal (SP) cyclization because the former produces a stable aromatic diradical, whereas the latter gives an unstable non-aromatic fulvene diradical^{33,57}. The present study revealed an unexpected cyclization route in addition to the classic Bergman cyclization (BC) and Schreiner–Pascal (SP) pathways. This path has lower activation energy, applicable to boryl groups with Cl, Br, and CN substituents, and leads to non-aromatic fulvene zwitterions through ionic- SP [NICS(1): ~ -1.0 ppm]. In contrast, the presence of moderately electrophilic boryl groups [$-\text{BH}_2$, $-\text{BF}_2$, and $-\text{B}(\text{OH})_2$] at C5 led to 6-endo BC products through the ionic mechanism. The hydroxy group of $-\text{B}(\text{OH})_2$ was particularly noteworthy, as it formed a ($3c-4e$)-hydrogen bond with the anionic center at C5 and stabilized the transition state. Additionally, polar solvents stabilized the reactant more than the transition state, increasing activation energy (Fig. S9 in SI)^{58–60}. Interestingly, the least electrophilic $-\text{B}(\text{NH}_2)_2$ generated

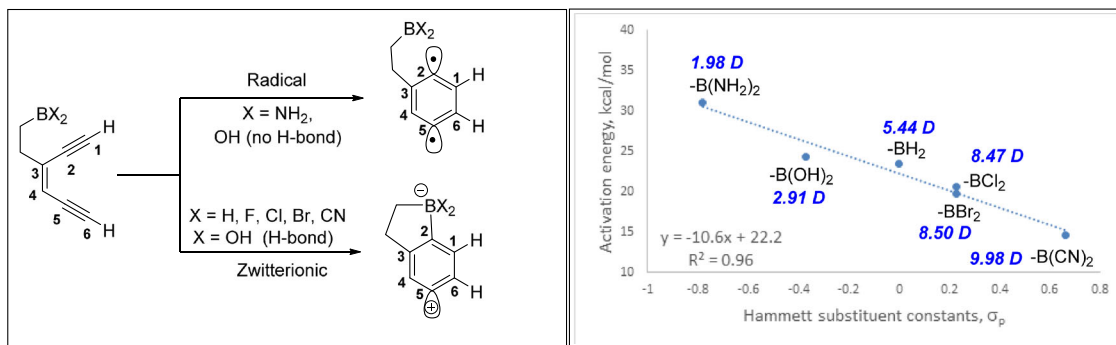


Fig. 9 The scheme on the left show two possible outcomes when enediyne containing electronically diverse boryl groups undergo BC. The plot on the right shows the dependence of activation energy on the electrophilicity of boryl groups. Values in blue font indicate the net dipole moment of the TS.

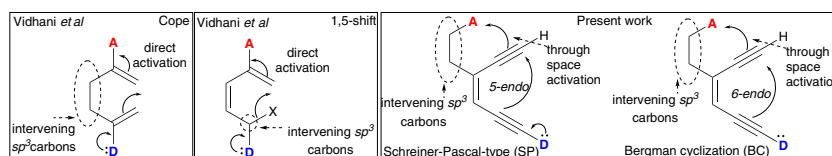


Fig. 10 FLP-mediated Cope, 1,5-sigmatropic shift, and ionic-Bergman cyclization. Groups A and D correspond acceptor and donor, respectively.

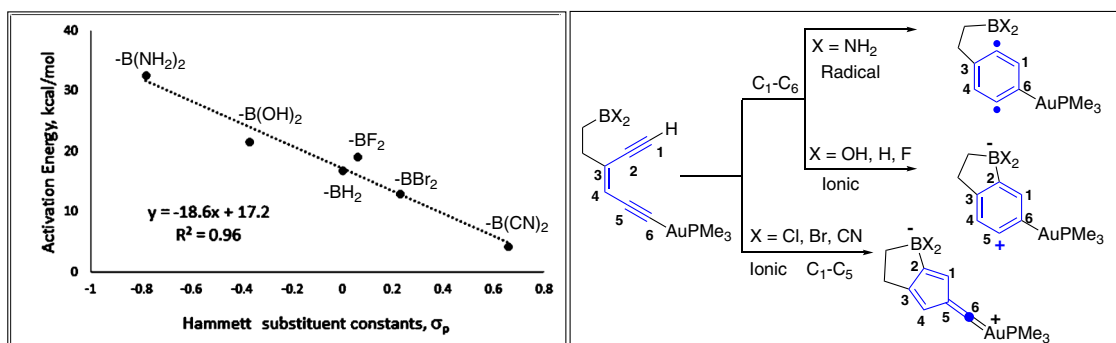


Fig. 11 The scheme on the right show three possible outcomes when enediyne contain both electronically diverse boryl groups and Au(I)-acetylides. The plot on the left shows the dependence of activation energy on the electrophilicity of boryl groups when Au(I)-acetylide contains PMe₃ ligand. All geometries were optimized at the B3LYP/LANL2DZ level.

1,4-diradical through the classic BC (Fig. 11). This diradical had relatively low activation energies, the ability to form a (3c-3e)-hydrogen bond, and TS geometry comparable to the BC of the parent enediyne and its boron analogs (B and D, Fig. 8). Unlike $-B(OH)_2$ system, the polar solvents only marginally increased the activation energy in the systems containing (3c-3e)-hydrogen bond. This was primarily due to greater stabilization of the reactant than the transition state, leading to a slight increase in activation energy when shifting from less polar to more polar solvents (Fig. S8 in SI).

Bergman cyclization of a broader range of substrates showed a strong correlation between Hammett's constants and the activation energies. Notably, the combination of $-BX_2$ and Au(I)PMe₃ revealed a steeper slope (-18.6 , Fig. 11) compared to boryl substrates without the σ -Au(I)PMe₃ (slope = -10.6 , Fig. 9). This was unexpected, as the σ -Au(I)PMe₃-acetylide had previously been inactive without boryl groups (Fig. 5). Consequently, the study of the combined effect of ligands on σ -Au(I) and substituents on the boryl groups revealed that, in general, ligands on Au(I) decreased the activation energy based on their strength, with anionic ligands having the most significant effect (7–10 kcal/mol, Fig. 12). The mechanism of cyclization was also affected, with $-B(OH)_2$, $-BH_2$, and $-BF_2$ groups undergoing a change from ionic-Bergman cyclization (i-BC) to ionic-

Schreiner–Pascal (i-SP) rearrangement when anions replaced the neutral ligands on Au(I) (Fig. 12). A similar mechanistic shift occurs when C5 contains highly electrophilic groups such as $-BCl_2$, $-BBr_2$, or $-BCN_2$. The least electrophilic $[-B(NH_2)_2]$ boryl group followed the r-BC pathway regardless of the ligand strength (Fig. 12).

The multivariate regression ($R^2 = 0.93$) depicted in Fig. 13 shows a linear correlation between the activation energy (z-variable) and two variables—the electrophilicity of the boryl group (x-variable) and the strength of ligand on σ -Au(I)-acetylide (y-variable). The electrophilicity of the boryl group was assessed by analyzing Hammett's constants of substituents attached to the boron atom, and the strength of the ligand was evaluated by comparing its binding affinity to Au(I) with that to water. The coefficients of the equation " $E_a = 18.1 - 18.9x - 0.042y$ ", obtained from fifty-five (55) substituted enediyne, showed the boryl groups had a larger impact on the activation energy than the ligands on Au(I). Furthermore, the multivariate plot revealed three distinct areas - r-BC, i-BC, and i-PS - delineated by the "Rubicon crossings," corresponding to the significant mechanistic shifts. The first mechanistic shift, "Rubicon—first crossing" occurs when the least electrophilic $-B(NH_2)_2$ group is replaced by the slightly more electrophilic $-B(OH)_2$, transforming r-BC into i-BC. The second shift,



		Strength of Ligand (Weak)  (Strong)							
		H ₂ S	P(OH) ₃	H ₂ O	P(NH ₂) ₃	PMe ₃	Br ⁻	Cl ⁻	F ⁻
Acidity of boron (Weak)  (Strong)	B(NH ₂) ₂	C ₁ -C ₆ 33.1 <i>r-BC</i>	C ₁ -C ₆ 33.3 <i>r-BC</i>	C ₁ -C ₆ 33.1 <i>r-BC</i>	C ₁ -C ₆ 33.4 <i>r-BC</i>	C ₁ -C ₆ 32.6 <i>r-BC</i>	C ₁ -C ₆ 28.9 <i>r-BC</i>	C ₁ -C ₆ 29.0 <i>r-BC</i>	C ₁ -C ₆ 29.2 <i>r-BC</i>
	B(OH) ₂	C ₁ -C ₆ 22.9 <i>i-BC</i>	C ₁ -C ₆ 23.5 <i>i-BC</i>	C ₁ -C ₆ 22.7 <i>i-BC</i>	C ₁ -C ₆ 22.1 <i>i-BC</i>	C ₁ -C ₆ 21.6 <i>i-BC</i>	C ₁ -C ₅ 13.8 <i>i-PS</i>	C ₁ -C ₅ 13.7 <i>i-PS</i>	C ₁ -C ₅ 13.3 <i>i-PS</i>
	BH ₂	C ₁ -C ₆ 18.9 <i>i-BC</i>	C ₁ -C ₆ 19.6 <i>i-BC</i>	C ₁ -C ₆ 18.4 <i>i-BC</i>	C ₁ -C ₆ 18.1 <i>i-BC</i>	C ₁ -C ₆ 16.3 <i>i-BC</i>	C ₁ -C ₅ 8.8 <i>i-PS</i>	C ₁ -C ₅ 8.7 <i>i-PS</i>	C ₁ -C ₅ 8.4 <i>i-PS</i>
	BF ₂	C ₁ -C ₆ 21.5 <i>i-BC</i>	C ₁ -C ₆ 22.1 <i>i-BC</i>	C ₁ -C ₆ 20.9 <i>i-BC</i>	C ₁ -C ₆ 19.8 <i>i-BC</i>	C ₁ -C ₆ 19.1 <i>i-BC</i>	C ₁ -C ₅ 10.5 <i>i-PS</i>	C ₁ -C ₅ 10.3 <i>i-PS</i>	C ₁ -C ₅ 9.9 <i>i-PS</i>
	BCl ₂	C ₁ -C ₅ 14.1 <i>i-PS</i>	C ₁ -C ₅ 14.7 <i>i-PS</i>	C ₁ -C ₅ 13.5 <i>i-PS</i>	C ₁ -C ₅ 13.0 <i>i-PS</i>	C ₁ -C ₅ 12.6 <i>i-PS</i>	C ₁ -C ₅ 6.4 <i>i-PS</i>	C ₁ -C ₅ 6.2 <i>i-PS</i>	C ₁ -C ₅ 5.8 <i>i-PS</i>
	BBr ₂	C ₁ -C ₅ 14.4 <i>i-PS</i>	C ₁ -C ₅ 12.8 <i>i-PS</i>	C ₁ -C ₅ 13.9 <i>i-PS</i>	C ₁ -C ₅ 13.4 <i>i-PS</i>	C ₁ -C ₅ 12.9 <i>i-PS</i>	C ₁ -C ₅ 6.8 <i>i-PS</i>	C ₁ -C ₅ 6.3 <i>i-PS</i>	C ₁ -C ₅ 5.8 <i>i-PS</i>
	B(CN) ₂	C ₁ -C ₅ 5.8 <i>i-PS</i>	C ₁ -C ₅ 6.2 <i>i-PS</i>	C ₁ -C ₅ 5.4 <i>i-PS</i>	C ₁ -C ₅ 4.6 <i>i-PS</i>	C ₁ -C ₅ 4.2 <i>i-PS</i>	C ₁ -C ₅ 0.0 <i>i-PS</i>	C ₁ -C ₅ 0.0 <i>i-PS</i>	C ₁ -C ₅ 0.0 <i>i-PS</i>

Fig. 12 Comparative study of showing the mode of cyclization and the activation energy as a function of electrophilicity of boryl groups and the strength of ligand on Au(I). Calculations were performed at the B3LYP/LANL2DZ level, and the activation energy is expressed in kcal/mol. The terms *i-BC*, *i-PS*, and *r-BC* denote ionic-Bergman cyclization, ionic Schreiner–Pascal cyclization, and radical Bergman cyclization, respectively. The C₁-C₆ and C₁-C₅ represent 6-endo and 5-endo modes of cyclizations, respectively.

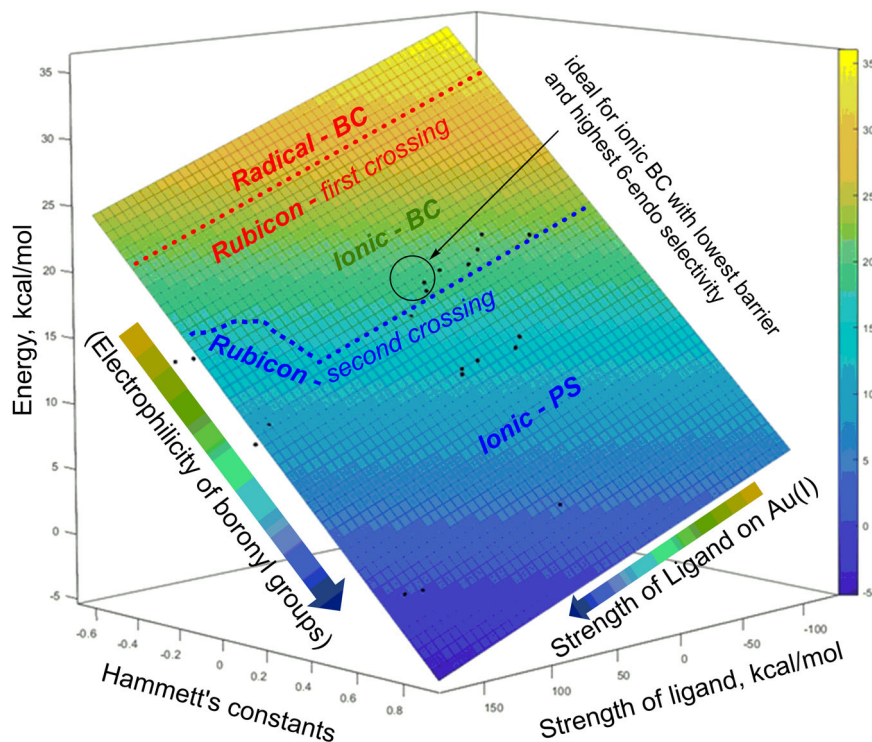


Fig. 13 Multivariate plot with 55 data points showing the dependence of activation energy (E_a) on the strength of ligand on Au(I) and the electrophilicity of the boryl group. “Rubicon—first crossing” in red font denotes a mechanistic shift from *radical-BC*→*ionic-BC*. “Rubicon—second crossing” in blue font indicates a mechanistic shift from *ionic-BC*→*ionic-PS*.

“Rubicon—second crossing,” highlights the influence of ligands on Au(I) and results in the transformation of *i-BC* into *i-PS*. All boryl groups, apart from -B(NH₂)₂, preferred the *i-PS* path when combined with anionic ligands (F, Cl, and Br) on Au(I). Moreover, highly electrophilic boryl groups also favor the *i-PS* pathway regardless of the ligand type present on Au(I). One of

the goals of this study was to identify a suitable combination of the boryl group and the ligand on Au(I) that will: (1) initiate the *i-BC* pathway, (2) have low activation energy, and (3) avoid undesired *i-PS*. The combination of -BH₂ and PMe₃ groups, as depicted in Fig. 13, meets these criteria effectively and triggers the intended cascade.

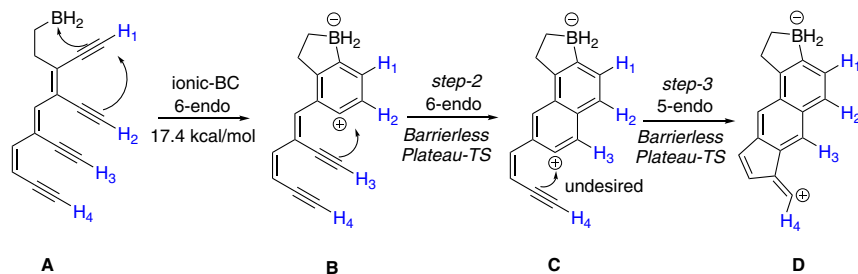


Fig. 14 Boryl group-triggered Bergman cascade resulting into the terminal five-membered fulvene-type cation. Structures **A**, **B**, **C**, and **D** correspond to the polyenyne substrate, phenyl cation, naphthyl cation, and the final product of cascade cyclization respectively. Calculations were performed using the B3LYP/LANL2DZ level.

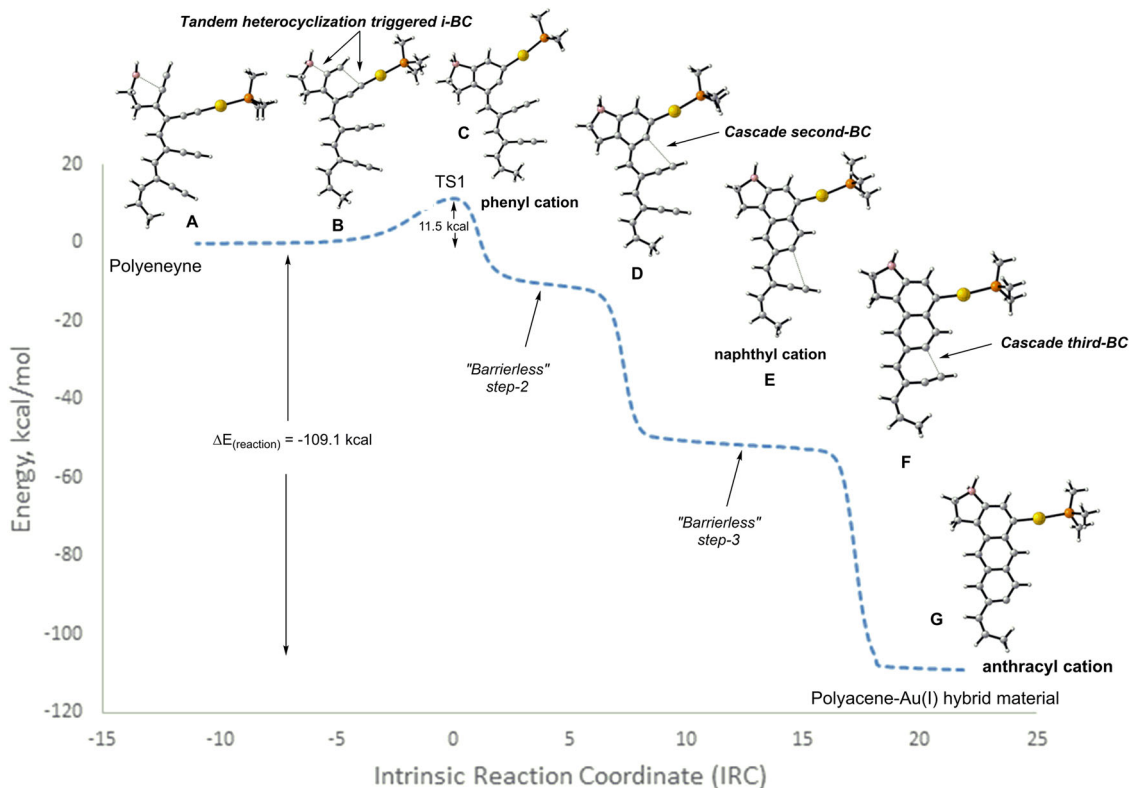


Fig. 15 Au(I)/BH₂ couple-triggered Bergman cascade resulting in an all-six-membered polyaromatic system. Structures **A**, **B** and **C** correspond to the acyclic polyenyne substrate, transition state and resulting phenyl cation from the ionic BC. Structures **D**, **E**, and **F** correspond to representative geometries in the barrierless regions of step-2 and step-3. Structure **G** corresponds to the anthracyl cation. Calculations were performed using the B3LYP/LANL2DZ level.

Cascade cyclizations: accessing TM-polyacene hybrid materials using *i*-BC. The Bergman cyclization of enediyne is a promising tool for generating carbon-rich materials such as carbon nanotubes and carbon-nano-ions^{61,62}. However, its utility in polymer and material sciences is limited due to its inherent drawbacks, such as the self-quenching of diradicals, the high reactivity of diradicals, and the unwanted 5-endo cyclization leading to fulvene radicals causing large polydispersities⁶¹. In this regard, our investigation of *i*-BC triggered by the Au(I)PMe₃/BH₂ couple provides a viable alternative for initiating a defect-free polymerization (Figs. 12, 13). To evaluate its effectiveness, we chose polyenynes with the potential to give three consecutive aromatic rings. Initially, we studied the effect of -BH₂ on the cascade reaction without Au(I)PMe₃. In this situation, the -BH₂ group initiated the *i*-BC reaction (17.4 kcal/mol, Fig. 14), creating two aromatic rings (B and C, Fig. 14). Surprisingly, the process ended with a 5-membered fulvene-type vinyl cation instead of a

6-membered aromatic ring (D, Fig. 14). In addition, the IRC analysis showed a notably exothermic cascade (−110 kcal/mol) in which steps 2 and 3 (B→C→D, Fig. 14) showed barrierless flat regions along the IRC. Mechanistically, these regions represent undefined intermediates B and C and their corresponding transition states (TS_{B→C} and TS_{C→D}, Fig. S5 in SI).

Remarkably, the utilization of BH₂/Au(I)PMe₃ couple in the polyenyne system yielded all six-membered rings with a low activation energy (E_a = 11.5 kcal/mol) and no undesired 5-endo cyclic unit (Fig. 15). The IRC analysis, once again, revealed an unusual trajectory along the PES, featuring barrierless steps for both the second and third cyclizations. The flat regions along the IRC indicate that the energies and geometries of the products of the first and second steps (C and E, Fig. 15) coalesce with that of the second and third transition states, respectively. The four-step cascade reaction generating an anthracene derivative is predicted to be highly exothermic (−109.1 kcal/mol), forming multiple

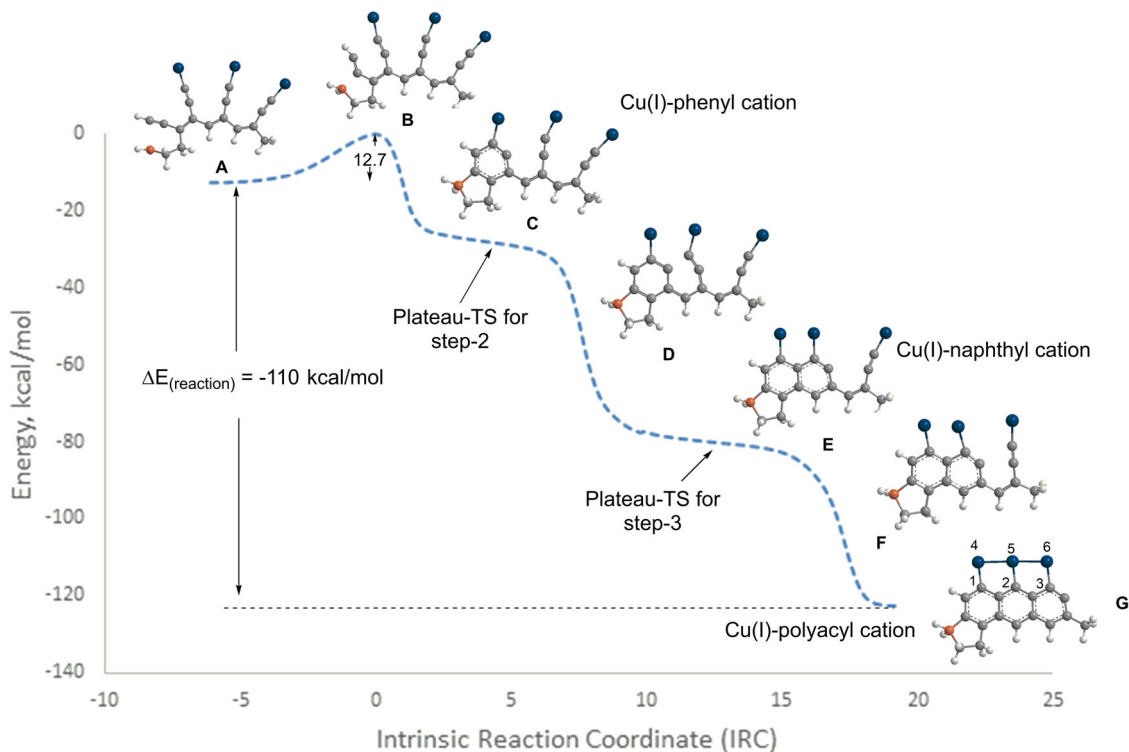


Fig. 16 Cu(I)/BH₂ couple-triggered Bergman cascade resulting in an all-six-membered polyaromatic system. Structures **A**, **B** and **C** correspond to the polyenyne acyclic substrate, transition state and resulting phenyl cation from the ionic BC. Structures **D**, **E**, and **F** correspond to representative geometries in the barrierless regions of step-2 and step-3. Structure **G** corresponds to the anthracyl cation. Calculations were performed using the B3LYP/LANL2DZ level.

aromatic rings contributing to the enormous reaction energy. This high reaction energy is consistent with the radical cascade process reported by ref. ⁶³. Interestingly, polar solvents reduce the activation energy to 9.8 kcal/mol compared to the gas phase (Fig. S10 in SI). Additionally, the free energy surface in acetonitrile was also similar to that of the gas phase (Fig. S11 in SI).

Curiously, extending this approach to BH₂/Cu(I) system produced two aromatic rings but terminated in an unwanted five-membered fulvene-type vinyl cation (Fig. S6 in SI). Replacing all hydrogens on alkynes by copper (I) produced the desired array of six-membered aromatic rings. The PES, low activation energy (12.7 kcal/mol), and a high exothermic effect (−110 kcal/mol) were also comparable with BH₂/Au(I)PMe₃ system (Fig. 16). The NBO interaction energies in poly-Cu(I) product **G** exhibited a significant degree of electron delocalization between the Cu(I) ions located in the peri-position and the polyacene framework, resulting in the Cu(I) ion distance being close to the FCC metallic bond distance of solid copper crystal (2.56 Å) (Fig. 16). Since copper has excellent conducting properties, and the GNRs are exceptional semiconductors, we anticipate these novel hybrid materials to possess unique electrical properties⁶⁴.

Finally, we assessed the bandgaps and reorganization energies of the TM-polyacene hybrid material to evaluate its semiconducting characteristics. To validate the reliability of the B3LYP/LANL2DZ level, we compared the calculated HOMO-LUMO gap with the experimental data of the unsubstituted polyacenes (Fig. S7 in SI). The values for ≥4 rings agreed with experimental data, only differing by 0.1–0.2 eV (Fig. 17). When applied to molecules with a smaller dielectric constant, such as benzene and naphthalene, the B3LYP calculations with a 20% Hartree-Fock exchange differed from experimental values by 0.5 eV. Since we were interested in larger polyacenes, and the B3LYP-calculated

trend agreed with the experimental results, we chose B3LYP to calculate the electronic properties of our Au(I) and Cu(I) hybrid systems⁶⁵. The bandgap of unsubstituted polyenyynes demonstrated an exponential decrease; however, the lowering is more substantial for metal-substituted polyacenes due to increased electron delocalization (Fig. 17). As reported by several groups, the transition metals, in these cases too, cause a more significant decrease in the energy of LUMO compared to the increase in the HOMO energy^{66–70}. The comparison of the bandgaps in unsubstituted anthracene (3.6 eV), Au(I)-anthracene (2.6 eV), and Cu(I)-anthracene (2.0 eV) further highlights this effect (Fig. 17). Interestingly, the bandgaps in the latter two complexes were within the acceptable range of wide-bandgap semiconductors such as pentacene (2.5 eV) which is extensively used in UV/Visible LEDs, LASERS, and various electronic devices⁷¹. For the TM-polyacenes with four or more aromatic rings, the bandgap exponentially approaches the limit of silicon-based semiconductors (1.1 eV).

Alongside HOMO-LUMO energies and bandgaps, the reorganization energy associated with charge transport is an essential factor in evaluating the performance of semiconductors. According to the Marcus theory, the rate of charge transport is inversely proportional to the reorganization energy. For p-type semiconductors such as anthracene, tetracene, and pentacene, the four-point model equation (Eq. 1) predicted the hole transport reorganization energies (λ_T^+) to decrease with the increasing number of aromatic rings (See Fig. S12 in SI)⁷². Additionally, the DFT-calculated values for the selected unsubstituted polyacenes were in excellent agreement with the experiments (Table 1)^{73–75}. Interestingly, the low reorganization energies, ranging from 0.1 to 0.2 eV, were predicted for gold and copper derivatives (Table 1). This trend suggests that TM-polyacene hybrid materials with small bandgap and low reorganization energies could be

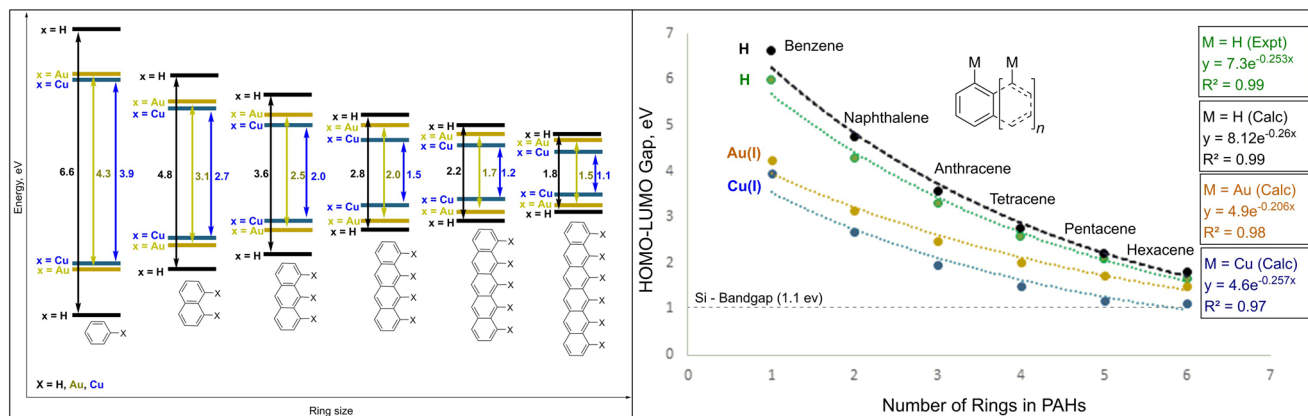


Fig. 17 Comparing the bandgaps of unsubstituted and transition metal-substituted polyacenes. Left: Bandgaps as a function of the number of rings in unsubstituted, Au(I)-substituted, and Cu(I)-substituted polyacenes. Right: Exponentially declining bandgaps as a function of the number of delocalized p-bonds in unsubstituted, Au(I)-substituted, and Cu(I)-substituted polyacenes. The green and black plots on the right correspond to experimental and DFT-calculated bandgap, respectively. All calculations were performed using the B3LYP/LANL2DZ level.

Table 1 Hole transport reorganization energies (λ_+) and bandgaps of selected polyacenes and their Au(I) and Cu(I) derivatives.

Compounds	Hole Transport λ_+ (eV)	Bandgaps (eV)
Anthracene	0.135 (0.138) ⁷³	3.560
Tetracene	0.108 (0.111) ⁷⁴	2.762
Pentacene	0.045 (0.05) ⁷⁵	2.206
Anthracene-Cu	0.201	1.965
Tetracene-Cu	0.190	1.504
Pentacene-Cu	0.189	1.183
Anthracene-Au	0.169	2.473
Tetracene-Au	0.150	2.030
Pentacene-Au	0.139	1.724

Energies are expressed in electron volts (eV). Values in parenthesis correspond to experimentally determined reorganization energies. All calculations were performed at the B3LYP/LANL2DZ level.

promising candidates for further experimental study.

$$\lambda_T^\pm = \lambda_1^\pm + \lambda_2^\pm \quad (1)$$

λ_T^\pm : Hole or electron transport reorganization energies

$$\lambda_1^\pm : E_{(\text{Neutral Geometry Vertical Ionization})}^\pm - E_{(\text{Optimized Geometry of ion})}^\pm$$

$$\lambda_2^\pm : E_{(\text{Ion Geometry Vertical Neutralization})}^0 - E_{(\text{Neutral Optimized Geometry})}^0$$

Concluding remarks

The present work provides a “bottom-up” substrate design to access TM-GNR hybrid semiconductors using zwitterionic Bergman cyclization-triggered cascade polymerization. These materials, exhibiting unusual optoelectronic properties, contain the thinnest semiconducting polyacene chain with a single-atom-thick metal wire. The first step towards accessing these materials was to design polyynes that can undergo zwitterionic BC while avoiding unwanted side reactions. To this end, most boryl groups lowered the activation energy and changed the nature of the intermediate from the diradical to zwitterionic at the Bergman cyclization (BC) stage. Notably, electron-rich $-B(NH_2)_2$ adopted the classical BC pathway despite the unusual (3c-3e)-hydrogen bond stabilizing the transition state. For $-B(OH)_2$, the hydroxy group forming a 3c-4e-hydrogen bond with C5 shifts the

mechanism from a high-energy radical BC to a lower-energy zwitterionic pathway. Further, the remotely placed boryl groups caused an unexpected activation of σ -Au(I)-acetylides, emphasizing the role of ligands on the transition metals in regulating zwitterionic BC. Multivariate analysis revealed the right combination of boryl group and ligands on Au(I)-acetylide that generated a low-barrier (16.3 kcal/mol) zwitterionic-BC with high 6-endo selectivity near the “Rubicon—Second Crossing.” Thus, boron-Au(I)L catalysis had key benefits over σ,π -dual-Au(I) catalysis, namely the ability to transform radical-BC to zwitterionic-BC, provide a low activation energy pathway, and limit the undesired 5-endo SP rearrangement. This combination initiated the cascade polymerization via zwitterionic-BC followed by a series of unusual barrierless reactions where the formation of subsequent rings involved several “structureless transitions,” leading to the desired polyacenes. To the best of our knowledge, this would be the first set of examples where such consecutive multiple barrierless plateau reactions were captured in the single IRC calculations. Finally, the Au(I) and Cu(I)-substituted polyacenes show great potential for use as semiconducting materials due to their bandgaps and reorganization energies comparable to those of larger unsubstituted pentacene. These compounds would be one of the smallest single-molecule semiconductors and ideal candidates for further exploration.

Methods

All geometries were optimized at the B3LYP/LANL2DZ levels, which frequently performs well for the transition metal compounds using Gaussian 03 program (see SI for reference)^{76–78}. For comparison, B3LYP/6-311+G**/def2-TZVP and PBE0/6-311+G**/def2-TZVP calculations were performed for the BC of unsubstituted enediyne and σ -Au(I)-acetylide systems^{33,37–40,45}. Furthermore, for comparison, B3LYP/6-311++G(d,p), PBE0/6-311++G(d,p), and PBE0/LANL2DZ calculations were performed for representative systems containing electronically diverse boryl groups. All IRC calculations were performed using B3LYP/LANL2DZ. Force Field calculation indicated that optimized structures were found to be true minima with no imaginary frequency. All energies have been expressed in hartrees and the frequencies in cm^{-1} .

Data availability

The authors declare that the data supporting the findings of this study are available within the paper [and its supplementary information files]. The cartesian coordinates of all species are deposited in Supplementary Data 1.

Received: 2 December 2022; Accepted: 24 March 2023;
Published online: 07 April 2023

References

- Mombeshora, E. T. et al. A review of graphene derivative enhancers for perovskite solar cells. *Nanoscale Adv.* **4**, 2057 (2022).
- Raad, S. H. & Atlasbaf, Z. Solar cell design using graphene-based hollow nanopillars. *Sci. Rep.* **11**, 16169 (2021).
- Adetayo, A. E., Ahmed, T. N., Zakhidov, A. & Beall, G. W. Improvements of organic light-emitting diodes using graphene as an emerging and efficient transparent conducting electrode material. *Adv. Opt. Mater.* **9**, 2002102 (2021).
- Savchenko, A., Yin, R. T., Kireev, D., Efimov, I. R. & Molokanova, E. Graphene-based scaffolds: fundamentals and applications for cardiovascular tissue engineering. *Front. Bioeng. Biotech.* **9**, 797340 (2021).
- Zakharova, O. V., Mastalygina, E. E., Golokhvast, K. S. & Gusev, A. A. Graphene nanoribbons: prospects of application in biomedicine and toxicity. *Nanomaterials* **11**, 2425 (2021).
- Jampilek, J. & Kralova, K. Advances in drug delivery nanosystems using graphene-based materials and carbon nanotubes. *Materials* **14**, 1059 (2021).
- Oliveira, A. M. L. et al. Graphene oxide thin films with drug delivery function. *Nanomaterials* **12**, 1149 (2022).
- Balqis, F., Prakoso, B., Hanif Hawari, N., Eldona, C. & Sumboja, A. Recent development of polyaniline/graphene composite electrodes for flexible supercapacitor devices. *Chem. Nano Mat.* **8**, e202200151 (2022).
- Zahir, N., Magri, P., Luo, W., Gaumet, J. J. & Pierrat, P. Recent advances on graphene quantum dots for electrochemical energy storage devices. *Energy Environ. Mater.* **5**, 201–214 (2021).
- Olabi, A. G., Abdelkareem, M. A., Wilberforce, T. & Sayed, E. T. Application of graphene in energy storage device – A review. *Renew. Sustain. Energy Rev.* **135**, 110026 (2021).
- Wang, X. Y., Narita, A. & Müllen, K. Precision synthesis versus bulk-scale fabrication of graphenes. *Nat. Rev. Chem.* **2**, 0100 (2018).
- Jolly, A., Miao, D., Daigle, M. & Morin, J. Emerging bottom-up strategies for the synthesis of graphene nanoribbons and related structures. *Angew. Chem.* **132**, 4652–4661 (2019).
- Moss, G. P., Smith, P. A. S. & Tavernier, D. Glossary of class names of organic compounds and reactivity intermediates based on structure (IUPAC Recommendations 1995). *Pure Appl. Chem.* **67**, 1307–1375 (1995).
- Zamoshchik, N., Zade, S. S. & Bendikov, M. Formation of acene-based polymers: mechanistic computational study. *J. Org. Chem.* **78**, 10058–10068 (2013).
- Zade, S. S. et al. Products and mechanism of acene dimerization. A computational study. *J. Am. Chem. Soc.* **133**, 10803–10816 (2011).
- Mondal, R., Adhikari, R. M., Shah, B. K. & Neckers, D. C. Revisiting the stability of hexacenes. *Org. Lett.* **9**, 2505–2508 (2007).
- Fudickar, W. & Linker, T. Why triple bonds protect acenes from oxidation and decomposition. *J. Am. Chem. Soc.* **134**, 15071–15082 (2012).
- Solà, M. Forty years of Clar's aromatic π -sextet rule. *Front. Chem.* **1**, 22 (2013).
- Bhattacharya, D., Panda, A., Misra, A. & Klein, D. J. Clar theory extended for polyacenes and beyond. *J. Phys. Chem. A* **118**, 4325–4338 (2014).
- Feng, X., Pisula, W. & Müllen, K. Large polycyclic aromatic hydrocarbons: synthesis and discotic organization. *Pure Appl. Chem.* **81**, 2203–2224 (2009).
- Roth, W. R., Hopf, H. & Horn, C. 1,3,5-Cyclohexatrien-1,4-diyl und 2,4-cyclohexadien-1,4-diyl. *Chem. Ber.* **127**, 1765–1779 (1994).
- Jones, R. R. & Bergman, R. G. p-Benzynes. Generation as an intermediate in a thermal isomerization reaction and trapping evidence for the 1,4-benzenediyl structure. *J. Am. Chem. Soc.* **94**, 660–661 (1972).
- Bergman, R. G. Reactive 1,4-dehydroaromatics. *Acc. Chem. Res.* **6**, 25–31 (1973). 1.
- Wang, K. K. Cascade radical cyclizations via biradicals generated from enediyne, enyne-allenes, and enyne-ketenes. *Chem. Rev.* **96**, 207–222 (1996).
- Zhou, Z. et al. Negative charge as a lens for concentrating antiaromaticity: using a pentagonal “defect” and helicene strain for cyclizations. *Angew. Chem. Int. Ed. Engl.* **59**, 1256–1262 (2019).
- Alabugin, I. V. & Gonzalez-Rodriguez, E. Alkyne origami: folding oligoalkynes into polyaromatics. *Acc. Chem. Res.* **51**, 1206–1219 (2018).
- Byers, P. M., Rashid, J. I., Mohamed, R. K. & Alabugin, I. V. Polyaromatic ribbon/benzofuran fusion via consecutive endo cyclizations of enediyne. *Org. Lett.* **14**, 6032–6035 (2012).
- Alabugin, I. V. et al. Radical cascade transformations of tris(o-aryleneethynyl)enes into substituted benzo[a]indeno[2,1-c]fluorenes. *J. Am. Chem. Soc.* **130**, 11535–11545 (2008).
- Byers, P. M. & Alabugin, I. V. Polyaromatic ribbons from oligo-alkynes via selective radical cascade: stitching aromatic rings with polyacetylene bridges. *J. Am. Chem. Soc.* **134**, 9609–9614 (2012).
- Hansmann, M. M., Tšupova, S., Rudolph, M., Rominger, F. & Hashmi, A. S. K. Gold-catalyzed cyclization of diynes: controlling the mode of 5-endo versus 6-endo cyclization—an experimental and theoretical study by utilizing diethynylthiophenes. *Chemistry* **20**, 2215–2223 (2014).
- Hansmann, M. M., Rudolph, M., Rominger, F. & Hashmi, A. S. K. Mechanistic switch in dual gold catalysis of diynes: C(sp³)-H activation through bifurcation-vinylidene versus carbene pathways. *Angew. Chem. Int. Ed. Engl.* **52**, 2593–2598 (2013).
- Schreiner, P. R., NavarroVazquez, A. & Prall, M. Computational studies on the cyclizations of enediyne, enyne-allenes, and related polyunsaturated systems. *Acc. Chem. Res.* **38**, 29–37 (2005).
- Vavilala, C., Byrne, N., Kraml, C. M., Ho, D. M. & Pascal, R. A. Jr. Thermal C1–C5 diradical cyclization of enediyne. *J. Am. Chem. Soc.* **130**, 13549–13551 (2008).
- dos Passos Gomes, G. & Alabugin, I. V. Drawing catalytic power from charge separation: stereoelectronic and zwitterionic assistance in the Au(I)-catalyzed Bergman cyclization. *J. Am. Chem. Soc.* **139**, 3406–3416 (2017).
- Undeela, S., Chandra, R., Nanubolu, J. B. & Menon, R. S. Gold-catalysed regioselective cascade cycloisomerisation reactions of aza-enediynes for the synthesis of substituted benzoisoquinoline derivatives. *Org. Biomol. Chem.* **17**, 369–373 (2019).
- Hirano, K. et al. Direct synthesis of fused indoles by gold-catalyzed cascade cyclization of diynes. *J. Org. Chem.* **76**, 1212–1227 (2011).
- Naoe, S. et al. Gold(I)-catalyzed regioselective inter-/intramolecular addition cascade of di- and triynes for direct construction of substituted naphthalenes. *J. Org. Chem.* **77**, 4907–4916 (2012).
- Vidhani, D. V. & Alabugin, I. V. Controlled evolution of the Cope rearrangement: transition from concerted to interrupted and aborted pericyclic reactions regulated by a switch built from an intramolecular frustrated Lewis pair. *J. Org. Chem.* **84**, 14844–14853 (2019).
- Vidhani, D. V., Krafft, M. E. & Alabugin, I. V. Gold(I)-catalyzed allenyl Cope rearrangement: evolution from asynchronicity to trappable intermediates assisted by stereoelectronic switching. *J. Am. Chem. Soc.* **138**, 2769–2779 (2016).
- Vidhani, D. V., Krafft, M. E. & Alabugin, I. V. Sterecontrolled synthesis of (E,Z)-dienes via tandem Rh(I)-catalyzed rearrangement of propargyl vinyl ethers. *Org. Lett.* **15**, 4462–4465 (2013).
- Vidhani, D. V., Cran, J. W., Krafft, M. E., Manoharan, M. & Alabugin, I. V. Gold(I)-catalyzed Claisen rearrangement of allenyl vinyl ethers: missing transition states revealed through evolution of aromaticity, Au(I) as an oxophilic Lewis acid, and lower energy barriers from a high energy complex. *J. Org. Chem.* **78**, 2059–2073 (2012).
- Vidhani, D. V., Gillett, J. R., Cusido, Y. & Alabugin, I. V. [1,5]-Sigmatropic shifts regulated by built-in frustration. *J. Phys. Chem. A* **124**, 6016–6028 (2020).
- Vidhani, D. V., Cran, J. W., Krafft, M. E. & Alabugin, I. V. Overriding the alkyneophilicity of gold: catalytic pathways from higher energy Au(i)-substrate complexes and reactant deactivation via unproductive complexation in the gold(i)-catalyzed propargyl Claisen rearrangement. *Org. Biomol. Chem.* **11**, 1624–1630 (2013).
- Cramer, C. J. Bergman, Aza-Bergman, and protonated Aza-Bergman cyclizations and intermediate 2,5-Arynes: chemistry and challenges to computation. *J. Am. Chem. Soc.* **120**, 6261–6269 (1998).
- Gräfenstein, J., Hjerpe, A. M., Kraka, E. & Cremer, D. An accurate description of the Bergman reaction using restricted and unrestricted DFT: stability test, spin density, and on-top pair density. *J. Phys. Chem. A* **104**, 1748–1761 (2000).
- Alabugin, I. V. & Manoharan, M. Radical-anionic cyclizations of enediyne: remarkable effects of benzannulation and remote substituents on cycloaromatization. *React. J. Am. Chem. Soc.* **125**, 4495–4509 (2003).
- Dong, H., Chen, B.-Z., Huang, M.-B. & Lindh, R. The Bergman cyclizations of the enediyne and its N-substituted analogs using multiconfigurational second-order perturbation theory. *J. Chem. Comp. Chem.* **33**, 537–549 (2011).
- Koga, N. & Morokuma, K. Comparison of biradical formation between enediyne and enyne-allene. Ab initio CASSCF and MRSDCI study. *J. Am. Chem. Soc.* **113**, 1907–1911 (1991).
- Navarro-Vázquez, A., Prall, M. & Schreiner, P. R. Cope reaction families: to be or not to be a biradical. *Org. Lett.* **17**, 2981–2984 (2004).
- Graulich, N., Hopf, H. & Schreiner, P. R. Heuristic thinking makes a chemist smart. *Chem. Soc. Rev.* **39**, 1503–1512 (2010).
- Graulich, N. The Cope rearrangement—the first born of a great family. *WIREs Comput. Mol. Sci.* **1**, 172–190 (2011).
- Moss, R. A., Platz, M. S., Jones, M. & Jones, M. *Reactive Intermediate Chemistry* (Wiley-Interscience, 2004).
- Valtazanos, P. & Ruedenberg, K. Bifurcations and transition states. *Theor. Chim. Acta* **69**, 281–307 (1986).
- Singleton, D. A. et al. Mechanism of ene reactions of singlet oxygen. A two-step no-intermediate mechanism. *J. Am. Chem. Soc.* **125**, 1319–1328 (2003).
- Hamaguchi, M., Nakaishi, M., Nagai, T., Nakamura, T. & Abe, M. Notable effect of an electron-withdrawing group at C3 on the selective formation of alkylenecyclobutanes in the thermal denitrogenation of 4-spirocyclopropane-1-pyrazolines. Nonstatistical dynamics effects in the denitrogenation reactions. *J. Am. Chem. Soc.* **129**, 12981–12988 (2007).

56. Ye, L., Wang, Y., Aue, D. H. & Zhang, L. Experimental and computational evidence for gold vinylidenes: Generation from terminal alkynes via a bifurcation pathway and facile C–H insertions. *J. Am. Chem. Soc.* **134**, 31 (2012).
57. Prall, M., Wittkopp, A. & Schreiner, P. R. Can fulvenes form from enediynes? A systematic high-level computational study on parent and benzannulated enediyne and enyne–allene cyclizations. *J. Phys. Chem. A* **105**, 9265–9274 (2001).
58. Varghese, J. J. & Mushrif, S. H. Origins of complex solvent effects on chemical reactivity and computational tools to investigate them: a review. *React. Chem. Eng.* **4**, 165 (2019).
59. McLennan, D. J. Semi-empirical calculation of rates of SN2 Finkelstein reactions in solution by a quasi-thermodynamic cycle. *Aust. J. Chem.* **31**, 1897 (1978).
60. Vayner, G., Houk, K., Jorgensen, W. L. & Brauman, J. I. Steric retardation of SN2 reactions in the gas phase and solution. *J. Am. Chem. Soc.* **126**, 9054 (2004).
61. Sun, Q. et al. On-surface formation of one-dimensional polyphenylene through Bergman cyclization. *J. Am. Chem. Soc.* **135**, 8448–8451 (2013).
62. Chen, S. & Hu, A. Recent advances of the Bergman cyclization in polymer science. *Sci. China Chem.* **58**, 1710–1723 (2015).
63. Byers, P. & Alabugin, I. V. Polyaromatic ribbons from oligo–alkynes via selective radical cascade: stitching aromatic rings with polyacetylene bridges. *J. Am. Chem. Soc.* **134**, 9609–9614 (2012).
64. Son, M. et al. Copper-graphene heterostructure for back-end-of-line compatible high-performance interconnects. *npj 2D Mater. Appl.* **5**, 41 (2021).
65. Shimazaki, T. & Nakajima, T. Application of the dielectric-dependent screened exchange potential approach to organic photocell materials. *Phys. Chem. Chem. Phys.* **18**, 27554–27563 (2016).
66. Heurich, J., Cuevas, J. C., Wenzel, W. & Schön, G. Electrical transport through single-molecule junctions: from molecular orbitals to conduction channels. *Phys. Rev. Lett.* **88**, 256803 (2002).
67. Tarakeshwar, P., Palacios, J. J. & Kim, D. M. Electrode–molecule interface effects on molecular conductance. *IEEE Trans. Nanotechnol.* **8**, 16–21 (2008).
68. Tsiapis, A. C. & Gkarbounis, D. N. Sequential metalation of benzene: electronic, bonding, magnetotropic and spectroscopic properties of coinage metalated benzenes studied by DFT. *J. Mol. Model.* **21**, 153 (2015).
69. Schmidbaur, H. & Raubenheimer, H. G. Excimer and exciplex formation in gold (I) complexes preconditioned by aurophilic interactions. *Angew. Chem. Int. Ed.* **59**, 14748–14771 (2020).
70. Harisomayajula, N. V. S., Makovetskyi, S. & Tsai, Y.-C. Cuprophilic interactions in and between molecular entities. *Chem. Eur. J.* **25**, 8936–8954 (2019).
71. Kitamura, M. & Arakawa, Y. Pentacene-based organic field-effect transistors. *J. Phys. Condens. Matter* **20**, 184011 (2008).
72. Marcus, R. Electron transfer reactions in chemistry. Theory and experiment. *Rev. Mod. Phys.* **65**, 599–610 (1993).
73. Aleshin, A. N., Lee, J. Y., Chu, S. W., Kim, J. S. & Park, Y. W. Mobility studies of field effect transistor structures based on anthracene single crystals. *Appl. Phys. Lett.* **84**, 5383–5385 (2004).
74. Goldmann, C. et al. Hole mobility in organic single crystals measured by a “flip-crystal” field-effect technique. *J. Appl. Phys.* **96**, 2080 (2004).
75. Kera, S. et al. Experimental reorganization energies of pentacene and perfluoropentacene: effects of perfluorination. *J. Phys. Chem. C* **117**, 22428–22437 (2013).
76. Soriano, E. & Marco-Contelles, J. Mechanistic insights on the cycloisomerization of polyunsaturated precursors catalyzed by platinum and gold complexes. *Acc. Chem. Res.* **42**, 1026–1036 (2009).
77. Felix, R. J., Xia, Y., Dudnik, A. S., Gevorgyan, V. & Li, Y. Mechanistic insights into the gold-catalyzed cycloisomerization of bromoallenyl ketones: Ligand-controlled regioselectivity. *J. Am. Chem. Soc.* **130**, 6940–6941 (2008).
78. Weber, D. et al. A gold-catalysed enantioselective Cope rearrangement of achiral 1,5-dienes. *Nat. Chem.* **4**, 405–409 (2012).

Acknowledgements

D.V.V. expresses immense gratitude to Dr. Jyrko Correa (Department Chair, MDC) for his active support and enthusiastic encouragement, which were the driving force behind the success of this research. D.V.V. would also like to show appreciation to Dr. Igor V. Alabugin (FSU) and Ms. Sudha for their insightful conversations, the High-Performance Computing (HPC) facility at FSU for their computer resources, Dr. Adrienne Thompson for helping make this manuscript accessible to the general audience, and Ms. Carla Hamaty (Former Chair) for her aid throughout the summer semester. Part of this research was funded by the National Science Foundation grant award: 1832436 (Building Capacity Hispanic Student Success from 2-year to 4-year Institutions through CUREs).

Author contributions

D.V. (MDC) is the principal investigator and the contributor to this research. R.U. (MDC) and T.S. (MDC) contributed to compiling the SI and revising the manuscript. M.M. (NFC) contributed to revising the manuscript and scientific contribution. D.V. (MDVS) contributed to revising the manuscript, including data analysis and preparing the digital work.

Competing interests

The authors declare no competing interests.

Additional information


Supplementary information The online version contains supplementary material available at <https://doi.org/10.1038/s42004-023-00866-w>.

Correspondence and requests for materials should be addressed to Dinesh V. Vidhani.

Peer review information *Communications Chemistry* thanks the anonymous reviewers for their contribution to the peer review of this work.

Reprints and permission information is available at <http://www.nature.com/reprints>

Publisher's note Springer Nature remains neutral with regard to jurisdictional claims in published maps and institutional affiliations.

 **Open Access** This article is licensed under a Creative Commons Attribution 4.0 International License, which permits use, sharing, adaptation, distribution and reproduction in any medium or format, as long as you give appropriate credit to the original author(s) and the source, provide a link to the Creative Commons license, and indicate if changes were made. The images or other third party material in this article are included in the article's Creative Commons license, unless indicated otherwise in a credit line to the material. If material is not included in the article's Creative Commons license and your intended use is not permitted by statutory regulation or exceeds the permitted use, you will need to obtain permission directly from the copyright holder. To view a copy of this license, visit <http://creativecommons.org/licenses/by/4.0/>.

© The Author(s) 2023